CORE
Metadata, citation and similar papers at core.ac.uk
Provided by Publications of the IAS Fellows

1971SoPh...17..218B

AN INSTRUMENT TO MEASURE ANISOTROPIES OF COSMIC RAY ELECTRONS AND PROTONS FOR THE EXPLORER 34 SATELLITE*

W. C. BARTLEY**, K. G. McCRACKEN†, U. R. RAO††, J. R. HARRIES‡, R. A. R. PALMEIRA, and F. R. ALLUM

The University of Texas at Dallas, Dallas, Texas, U.S.A.

(Received 20 October, 1970)

Abstract. An instrument to measure the anisotropy and energy spectra of cosmic-ray electrons and protons, and X-rays of solar and galactic origin is described. Such instruments were launched on 24 May, 1967 and 21 June, 1969 as component parts of the scientific payloads of the Explorer 34 and 41 satellites. A general description and the main characteristics of the detectors are presented and the stability of the instrument on Explorer 34 over its 23 months of operation is discussed. The method of analysis of the obtained angular distribution of solar cosmic ray particles in the ecliptic plane is given. It is shown that the anisotropy of low energy particles of solar origin decreases sharply to a very small value when the satellite penetrates the magnetosphere.

1. Introduction

Large number of particle observations made by sensitive detectors on board various space probes during the last few years support the hypotheses that the generation of energetic particles is a very common feature of all solar flares. Thus, the frequency of solar proton and electron events detected has increased greatly with the increase in the sensitivity of the detectors. Low energy proton events (<10 MeV) often exhibit very complicated time profiles which depend both on the injection pattern at the source and on the propagation in the interplanetary medium. Propagation effects become increasingly important as we consider particles of lower energy where the gyroradii become comparable to the scale size of small scale field irregularities. To investigate the complex phenomena involved it becomes necessary to increase the range of energies of particles detected (particularly at the low energy end of the spectrum), and to measure proton, electron and solar X-ray data concurrently from the same satellite.

Recent improvement in detection techniques has made it possible to measure relativistic and subrelativistic electrons of solar origin; and electrons have been detected even from quite small solar flares (e.g., importance 1). Since the propagation of electrons in the interplanetary medium, like that of ions, is strongly controlled by

* This work was supported by the National Aeronautics and Space Administration Grant NASr-198 and Contract NAS5-9075.

** Now at the National Academy of Sciences, Washington, D.C., U.S.A.
† Now at the Division of Mineral Chemistry, CSIRO, Box 124, Port Melbourne, Australia.
†† Now at the Physical Research Laboratory, Ahmedabad, India.
‡ Now at the University of Adelaide, Adelaide, Australia.

Solar Physics **17** (1971) 218–240. *All Rights Reserved*
Copyright © 1971 *by D. Reidel Publishing Company, Dordrecht-Holland*

© Kluwer Academic Publishers • Provided by the NASA Astrophysics Data System

1971SoPh...17..218B

the structure of the interplanetary magnetic field irregularities, the study of their anisotropies will add to our knowledge of the solar system magnetic fields.

Taking advantage of the advances in instrumentation technology, detectors were flown on the Explorer 34 and 41 (IMP F & G) satellites* to obtain detailed information on the time dependence, degree of anisotropy and spectral properties of the radiation responsible for various types of cosmic ray enhancement. The IMP Explorer series was particularly suitable for these experiments since each spacecraft spends over 70% of its time in the interplanetary medium and also because the spacecraft is spin-stabilized with its spin axis nearly normal to the ecliptic plane. The advantages of choosing a spin stabilized vehicle for anisotropy measurements are described in detail by Bartley *et al.* (1967a). Since the details on the configuration and operation of these instruments and the data which they return from both interplanetary space and within various regions of the Earth's magnetosphere will be the basis for a number of subsequent scientific papers, we provide here a detailed description of the instrument.

Charged particle detectors similar in general principle to the one herein described were flown by The University of Texas at Dallas (then the Southwest Center for Advanced Studies) on the Pioneer 6 and 7 (Bartley *et al.*, 1967a) and Pioneer 8 and 9 (Bukata *et al.*, 1970) deep-space probes.

2. Charged Particle Telescope

The University of Texas at Dallas (UTD) instrument on Explorer 34 utilizes a four element particle telescope and a proportional counter to provide energy spectrum and anisotropy information for 0.7–125 MeV protons, 0.07–27.0 MeV electrons, and >2 keV X-rays. The arrangement of the four elements of the composite telescope is displayed in Figure 1. A 300 μ totally depleted solid state detector, A, with sensitive area of 1.0 cm^2, is mounted in front of a plastic scintillator, B. The logic $A\bar{B}$ is employed to identify those particles which come to the end of their range in the solid state detector, corresponding to a maximum energy of 7 MeV for a proton incident normal to the surface of the detector. The logic AB is also employed to study those particles which penetrate the solid state detector and are registered by the B scintillator. A normally incident proton of energy <100 MeV will come to the end of its range in the third main element, a 10 g cm^{-2} CsI(Tl) scintillator, C. The fourth element, a cylindrical cup veto counter, D, indicates whether a particle ends its range in C ($BC\bar{D}$ logic). The use of the $BC\bar{D}$ logic also enables the identification of protons and electrons which come to the end of their ranges in the C crystal. In the proton mode of operation the threshold level in the B detector is set sufficiently high so that only particles with ionization losses much greater than the minimum are detected. At the

* Explorer 34 was launched from the Western Test Range, California, at 1406 UT on 1967, May 24, into a highly eccentric orbit of initial apogee 2.11×10^5 km, perigee 248 km, inclination 67.4°, and period 4 days, 7 hr, 45 min. An identical instrument was launched on board Explorer 41 on 1969, June 21.

© Kluwer Academic Publishers • Provided by the NASA Astrophysics Data System

1971SoPh...17..218B

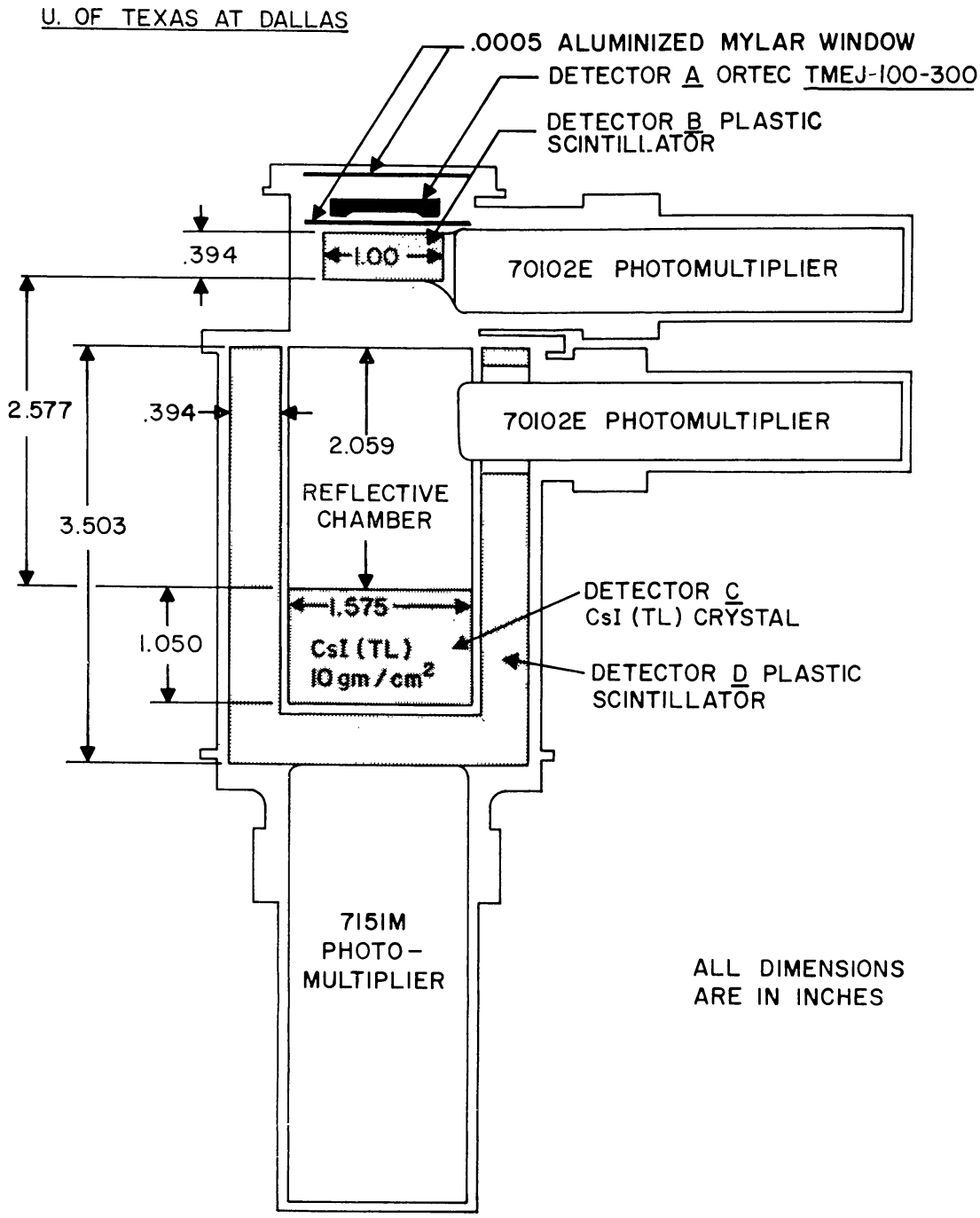

Fig. 1. Detailed view of the cosmic ray anisotropy detector for the Explorer 34 and 41 satellites.

same time, an attenuator is used in the output of the *C* crystal, so that only particles that deposit more than 30 MeV in the crystal are accepted. In the electron mode of operation, the threshold for the *B* scintillator is set such that only particles with ionization losses near the minimum are counted. Concurrently, the attenuator in the *C* crystal output is removed, so that energy losses greater than 1 MeV in the *C* crystal can be detected.

The plastic scintillator, *B*, is coupled to a 0.75 in. photomultiplier by an 'adiabatic'

© Kluwer Academic Publishers • Provided by the NASA Astrophysics Data System

1971SoPh...17..218B

light coupling manufactured from lucite. Both the scintillator and the light pipe are aluminized. The solid state detector, *A*, is separated from the scintillator, *B*, by an opaque barrier of 0.5×10^{-3} in. thick aluminized mylar. Two layers of similar aluminized mylar protect the solid state detector from direct sunlight in space and from thermal shock during the initial stages of the satellite launch when severe aerodynamic heating of the nearby fairing occurs. The solid state detector has been mounted with its '*N*' side (i.e., its ohmic aluminum contact) facing outwards to minimize proton radiation damage based on arguments presented by Coleman *et al.* (1968).

The light pulse from the CsI scintillator, *C*, aluminized on the back and sides, is viewed by an 0.75 in. photomultiplier via a light integrating chamber, the walls of which are brightly polished aluminum. Pulse height analysis is employed to indicate the energy deposited by each particle in the CsI scintillator. A 10 nanocurie Am^{241} radioactive source is attached to the CsI crystal to provide an inflight energy calibration. Laboratory measurements of the resolution of the CsI crystal response to the 5.5 MeV alpha particles from the Am^{241} source yielded a value of 45% to the full width at half maximum (FWHM) of the pulse height distribution.

The light pulse from the veto counter, *D*, is viewed by a 1.5 in. photomultiplier in optical contact with the scintillator. Aluminum foil is employed in the present experiment as a specular reflector, consistent with tests (Bartley *et al.*, 1967a) on a similar cup-shaped veto counter that favor a non-wetting reflecting material totally surrounding an optically polished scintillator.

The geometrical factors and cones of acceptance for various coincidence and anti-coincidence logics are given in Table I.

TABLE I

Particle telescope cones of acceptance and geometrical factors for The University of Texas at Dallas detector on Explorer 34

Logic	Maximum cone (half angle)	Geometric factor
BCD	26.5°	1.3 cm^2 ster
AB	68°	3.0 cm^2 ster
AB	68°	3.0 cm^2 ster
Proportional counter[a]	2.5° × 60°	0.18 cm^2 ster

[a] As mentioned in the text, electron scattering in the collimator could double the solid angle from that expected if there were no scattering.

3. Proportional Counter

The proportional counter and collimator are sketched in Figure 2. The proportional counter is filled with 90% xenon and 10% methane (by volume) at a pressure of one

© Kluwer Academic Publishers • Provided by the NASA Astrophysics Data System

1971SoPh...17..218B

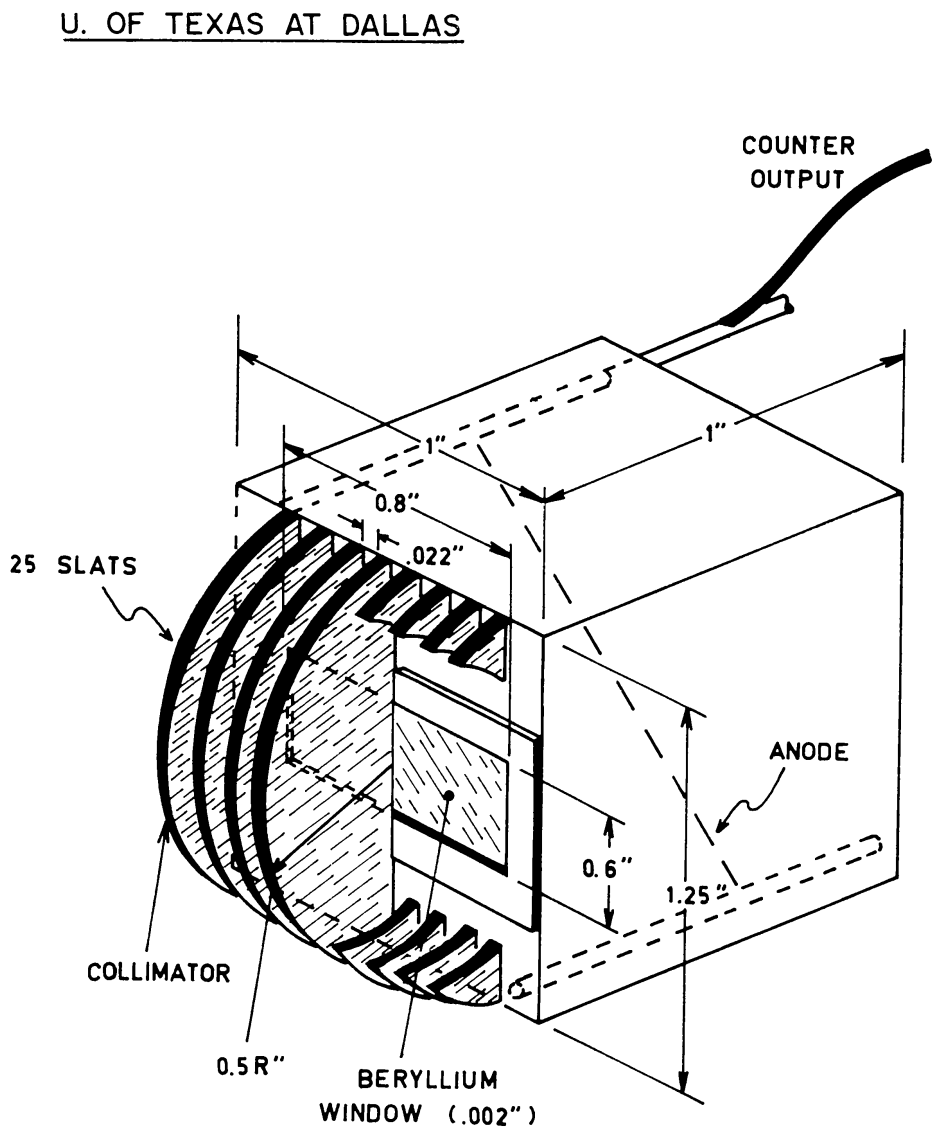

Fig. 2. Detailed view of the proportional counter and collimator for the Explorer 34 and 41 satellites.

atmosphere, and has a 0.6 in. by 0.8 in. and 2 mil thick beryllium foil window. The counter is 1.0 in. by 1.25 in. by 1.0 in. deep with an anode wire 0.0006 in. in diam. supported diagonally across the counter 0.5 in. behind the window. This configuration has been found to minimize the end effects for such a small counter while at the same time avoiding the problems experienced with point counters at low counting rates. The detector's gain is constant within 20% over the total window area, and the overall resolution for 5.9 keV X-rays from an Fe^{55} source was found to be 30% FWHM. The 1.5 keV fluorescent X-ray emission from the aluminum material of the collimator and counter walls falls below the 2.7 keV electronic threshold of the counter.

The transmission coefficient for electrons incident on the beryllium window is 10% at 70 keV and increases to 90% at 95 keV. The majority of the electrons that penetrate the window will deposit more than the 2.7 keV threshold set by the electronics, so

© Kluwer Academic Publishers • Provided by the NASA Astrophysics Data System

1971SoPh...17..218B

that the efficiency for detection of electrons is closely equal to the window transmission coefficient. Minimum ionizing electrons deposit >10 keV in the counter. For protons, the detection efficiency is also wholly determined by the beryllium window transmission coefficient, giving a detection threshold of 2.1 MeV. Protons with energies >17 MeV can penetrate the walls of the counter.

The X-ray detection efficiency is dependent both on the transmission through the beryllium window and the absorption in the xenon gas. The calculated X-ray detection efficiency for the proportional counter on Explorer 34 is shown in Figure 3.

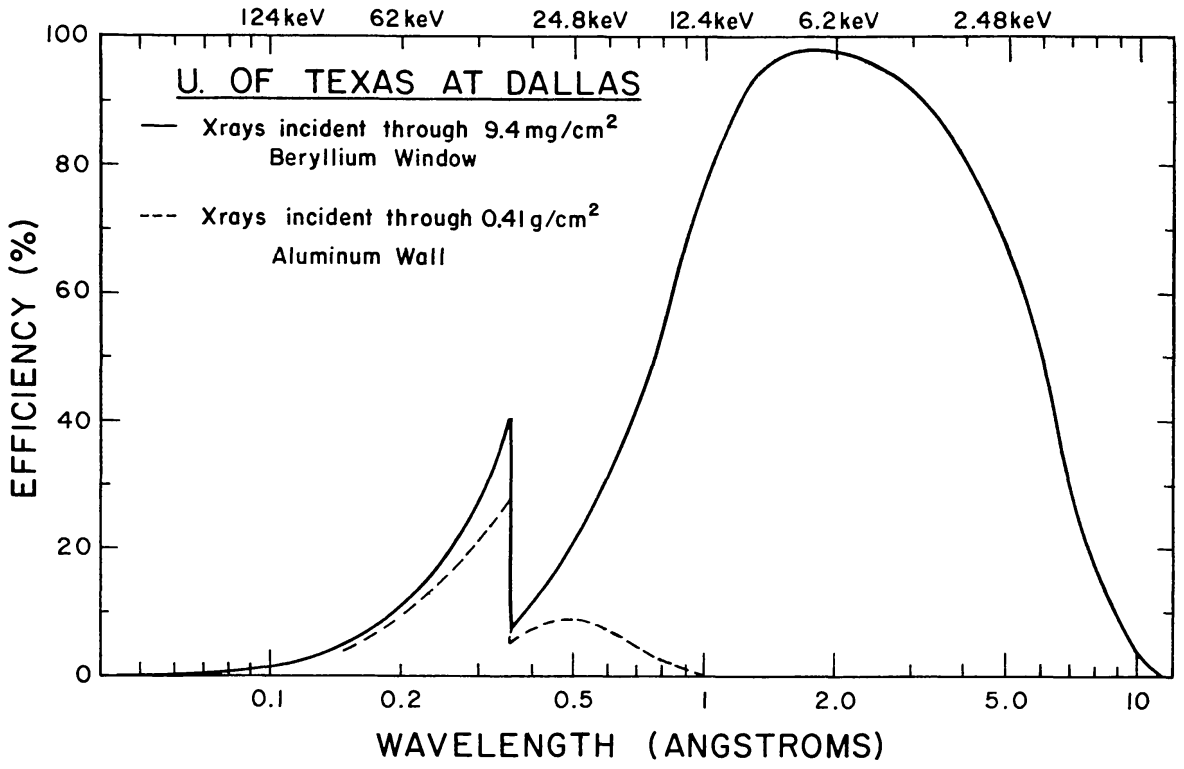

Fig. 3. The calculated detection efficiency of the proportional counter as a function of the incident X-ray wavelength.

The collimator in front of the proportional counter limits the field of view to 5° full opening angle in the ecliptic plane, however the response of the collimator to electrons is modified by the grazing incidence scattering of electrons on the sides of the aluminum slats (Kanter, 1957). This increases the opening angle of the collimator so that, for electrons, the 5° full width triangular response has a 'tail' which extends out to about 30° where it is less than one percent of the response at normal incidence. The scattering in the collimator could double the solid angle from that expected if there was no scattering. The field of view normal to the ecliptic is approximately 120°.

The collimator slats are semicircular with a radius of 0.5 in. as shown in Figure 2. The semicircular design compensates for the decrease in the projected area of the counter window for point sources above or below the ecliptic by giving a longer

© Kluwer Academic Publishers • Provided by the NASA Astrophysics Data System

1971SoPh...17..218B

period for the accumulation of counts. Hence the flux from X-ray sources can be measured without requiring the position of the source to be known. For charged particles a similar effect occurs and flux components above or below the ecliptic are given an equal weight with those wholly in the ecliptic plane.

In the anisotropy measurement, the proportional counter provides data on solar X-rays, electrons and protons. The electrons and protons are differentiated by comparing the response of the proportional counter to that of the solid state detector. The solar X-rays are identified by their direction of arrival.

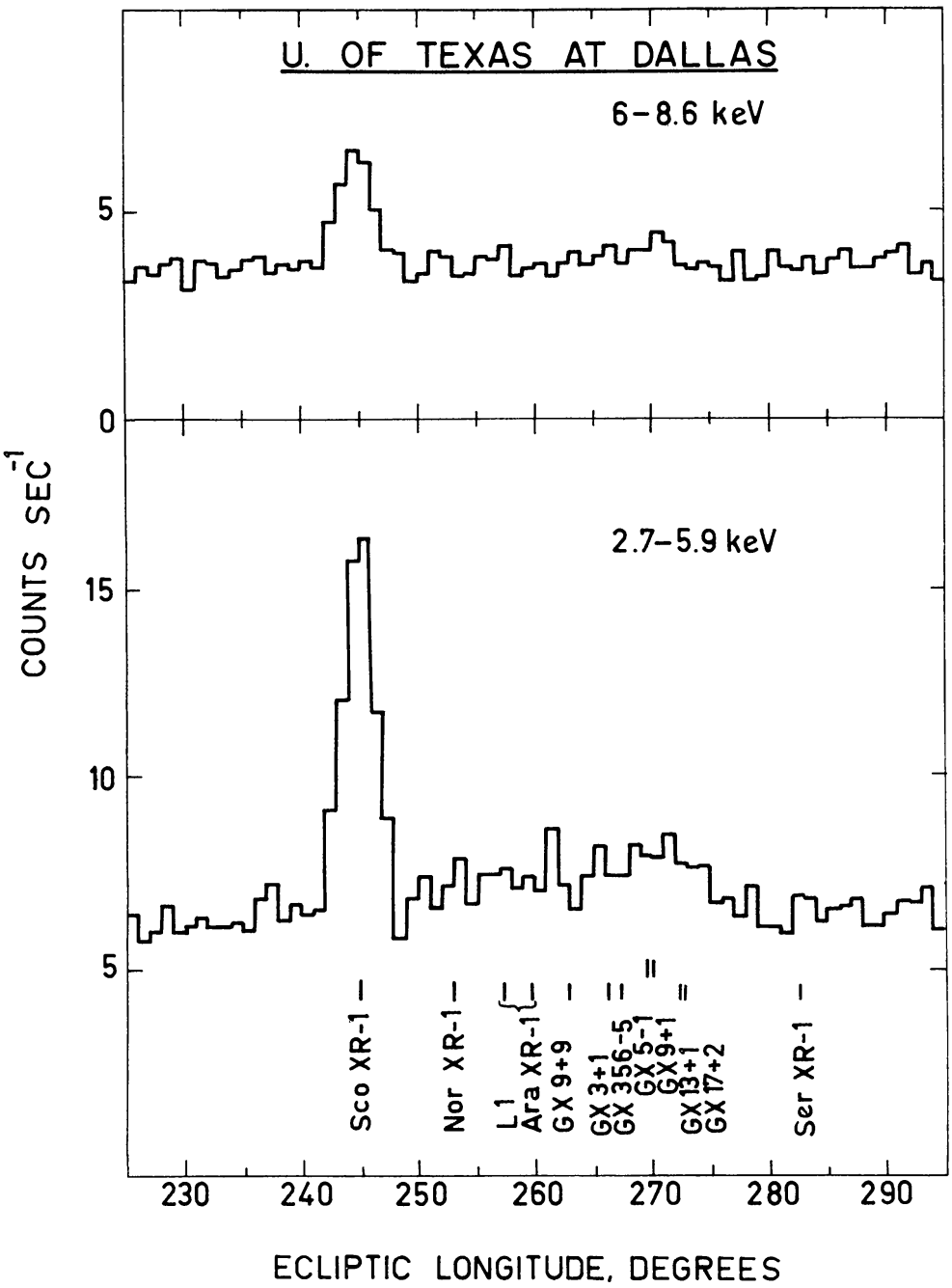

Fig. 4. The proportional counter responce for the source Sco XR-1 resulting from azimuth data accumulation during June and July 1967.

© Kluwer Academic Publishers • Provided by the NASA Astrophysics Data System

1971SoPh...17..218B

Celestial X-rays are observed in the azimuth measurement, where the output is pulse height analyzed into two energy channels, 2.7 to 5.9 keV and 6.0 to 8.6 keV. In this mode the experiment is relatively insensitive to low energy charged particles since only those particles that could penetrate the beryllium window and deposit less than 8.6 keV in the counter are accepted. This is equivalent to specifying an energy interval of 1 keV at 80 keV for electrons and less than 1 keV at 2.1 MeV for protons. In the azimuth measurement the spacecraft azimuth is determined with respect to the Sun at the instant when a pulse is observed in one of the pulse height analyzer channels. The azimuth is measured to an accuracy of 1.4° and four azimuth determinations are made every 81.92 sec. X-rays from the direction of the Sun are not analyzed in the azimuth measurement.

Celestial X-ray sources appear when data are accumulated for several days. Figure 4 shows the response from source Sco XR-1 resulting from the azimuth accumulations over June and July 1967.

4. Energy Discrimination

The outputs from the particle telescope are fed into a pulse height analyzer which provides 6 contiguous differential pulse height channels and an integral channel. The nominal energy limits of the several channels are indicated in Table II. A single seven channel pulse height analyzer is used in all operating modes, as indicated in simplified form in Figure 5. The pulses from the detectors (A and C) are first amplified by charge integrating amplifiers (Q-AMPs), then by a stage of voltage amplification. The

TABLE II

Energy intervals for The University of Texas at Dallas experiment on Explorer 34

Energy intervals for anisotropy measurements (MeV)

$L=0$	$L=1$	$L=2$	$L=3$	$L=4$	$L=5$		
Protons	Protons	Protons	Protons	Protons	Protons	Electrons	X-Rays
0.7–7.6	31.5–40	40–64	64–125	7.6–55	>2	>0.07	>0.002

Energy intervals for isotropy measurements (MeV)

Data accumulator	$L=6$ protons	$L=7$ even protons	$L=7$ odd electrons
SCA-1	31.5–35	0.7–1.1	2.8–3.3
SCA-2	35–40	1.1–1.6	3.3–4.0
SCA-3	40–46	1.6–2.3	4.0–4.8
SCA-4	46–64	2.3–3.5	4.8–7.2
SCA-5	64–100	3.5–7.6	7.2–11.3
SCA-6	100–125		11.3–16.0
SCA-7			16.0–27.0

© Kluwer Academic Publishers • Provided by the NASA Astrophysics Data System

1971SoPh...17..218B

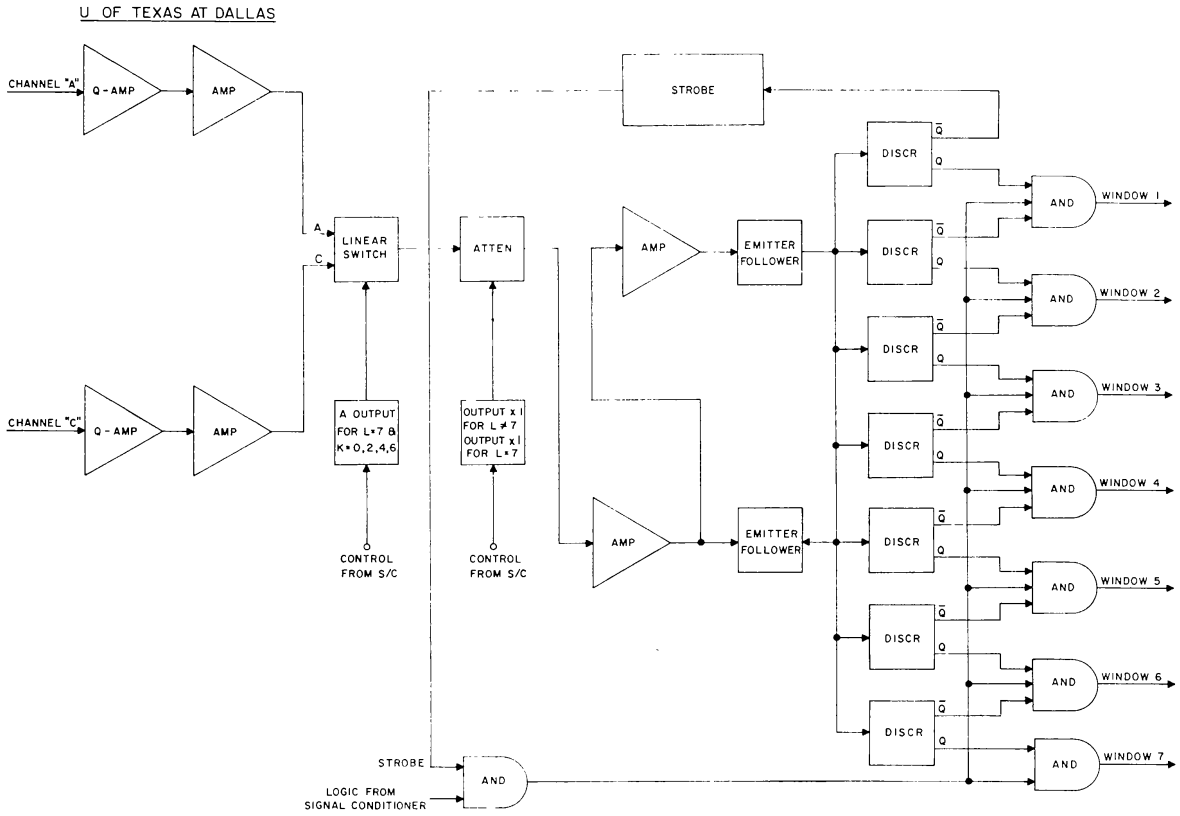

Fig. 5. Schematic block diagram of the 7-channel pulse height analyzer used in The University of Texas at Dallas experiment on the Explorer 34 and 41 satellites.

two signal amplifiers are connected to a linear switch, which transmits the appropriate input as determined by the current position in the experiment subcommutation cycle.

The pulse height analysis is achieved using the seven threshold discriminators D_1 through D_7. The Q output of the Nth discriminator (D_N), and the $\bar{Q}$ output of D_{N+1} are applied to an AND gate, along with a 'strobe' pulse (common to all AND gates). The strobe pulse is generated once the appropriate logic (e.g., electrons, calibrate, etc.) has been satisfied and is then delayed to prevent the detection of 'sneak' pulses due to the finite risetime of the input pulses. The resolution time for incoming pulses is 1μ sec.

5. Data Accumulation and Subcommutation

The output pulses from the various detection systems are counted and stored in separate binary accumulators provided by the spacecraft. Eight 10 bit counters identified SCA 1 through 8) are employed to record the counting rates from 8 different directions while in an 'anisotropic' mode (described below), and to record the rates from the seven pulse height analyzer windows when in an 'isotropic' mode (described below). The ninth, SCA 9, is a 10 bit counter employed to record the raw rates from the four detectors, A, B, C, and D, and to record on the data azimuth of the spacecraft at the time the proportional counter generates a pulse (sensing of pulses is inhibited

© Kluwer Academic Publishers • Provided by the NASA Astrophysics Data System

1971SoPh...17..218B

during octant 4, to be defined below, as the counter's response is almost exclusively due to solar X-rays at this time). The tenth, SCA 10, is a 6-bit counter used for housekeeping data essential to the interpretation of the anisotropy data from the particle telescope. Information in this 6-bit scaler, called 'START/STOP' data, is considered as two independent 3-bit data words; hence, the 96 data bits are efficiently divided among a total of eleven data words.

The Explorer 34 accumulators assigned to the UTD experiment are read out to Earth via real time telemetry every 10.24 sec. A period of 0.96 sec is occupied by the telemetry readout and accumulator reset, leaving 9.28 sec in each readout when pulses

TABLE III
SUBCOMMUTATION SCHEDULE FOR THE UNIVERSITY OF TEXAS AT DALLAS EXPERIMENT ON EXPLORER 34

L = →		0	1	2	3	4	5	6	7
LOGIC →		$A\bar{B}$	← $BC\bar{D}$ →			AB	PROP. COUNTER	$BC\bar{D}$	SEE BELOW
ENERGY RANGES (MeV)		0.7-7.6	31.5-40	40-64	64-125	7.6-55	> 2.0p > 0.07e > 0.002 XRAYS	SEE TABLE II	SEE TABLE II
0	SCA 1-8								$A\bar{B}$
1	SCA 1-8								$BC\bar{D}$
2	SCA 1-8								$A\bar{B}$
3	SCA 1-8								$BC\bar{D}$
4	SCA 1-8								$A\bar{B}$
5	SCA 1-8								$BC\bar{D}$
6	SCA 1-8								$A\bar{B}$
7	SCA 1-8								CALIB
K ↕	ACCUMULATOR ↕	← ANISOTROPIC MODE →						ISOTROPIC MODE ← →	
0-7	SCA 9	A RAW	B RAW	C RAW	D RAW	PROP. COUNTER AZIMUTH	PROP. COUNTER AZIMUTH	PROP. COUNTER AZIMUTH	PROP. COUNTER AZIMUTH
0-7	SCA 10	START STOP	START STOP	START STOP	START STOP	START STOP	START STOP	OCTANTS TOTAL	K

OMNIDIRECTIONAL COUNTS - ELECTRONS FROM TELESCOPE (SPECTRA)

DIRECTIONAL COUNTS - PROTONS FROM TELESCOPE

OMNIDIRECTIONAL COUNTS - PROTONS FROM TELESCOPE (SPECTRA)

DIRECTIONAL COUNTS - FROM PROPORTIONAL COUNTER

© Kluwer Academic Publishers • Provided by the NASA Astrophysics Data System

1971SoPh...17..218B

may be counted. A 'freeze' and a 'pre-freeze' (i.e. warning) pulses from the spacecraft system, occurring at the appropriate times, are used to inhibit data accumulation for short periods immediately after the start and just before the end of the 9.28 sec period, thus assuring equal accumulation times for all directional measurements. It is important to note that data acquisition must be Sun synchronous when anisotropies are being measured, as will be described later.

The UTD experiment subcommutates through a 64 position subcommutation cycle corresponding to 64 spacecraft readouts (10.92 min). During the 0.96 sec 'freeze' period, the experiment changes to provide a different type of measurement (e.g., different logic or energy level). Table III shows the subcommutation schedule. Reading across the schedule it will be noted that the experiment spends 61.44 sec in an 'anisotropy' mode, then switches to an 'isotropic' mode for 20.48 sec, and obtains 7 channel energy spectra of each of the two energy ranges 31.5–125 MeV and 0.7–7.6 MeV. Every second measurement of the 0.7–7.6 MeV proton spectrum is deleted, and an energy spectrum of electrons in the energy range 2.8–27 MeV is inserted instead. The experiment continues to cycle through the 'anisotropic' and 'isotropic' modes every 81.92 sec, thereby providing information on the temporal changes which occur in both the anisotropic and the isotropic flux of the cosmic radiation. Finally, the last measurement in the commutation cycle is a calibration mode during which the response of the CsI crystal to the Am^{241} source is recorded.

The nine 10-bit spacecraft accumulators are wired in an *S–T* (Signal/Time) logic configuration to provide sufficient dynamic range to cope with high particle fluxes (Figure 6); the 6-bit scaler is a standard binary counter of *S* (Signal) logic. The *S–T*

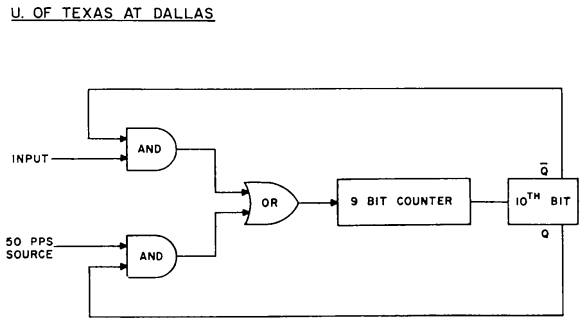

Fig. 6. Schematic block diagram of the 10-bit *S–T* type accumulators employed in the Explorer 34 and 41 satellites.

scaler used in our experiment counts pulses applied to the input in a normal fashion up to a decimal content of 511. The 512th pulse inserts a one into the 10th bit, and this closes the pulse input gate and opens a 50 pps input gate to the same counter. The counter thereafter will count time pulses for the remainder of the 9.28 sec data sampling interval. Hence, at high flux rates, when the 10th bit is a one, the actual pulse rate is given by $512/(9.28–0.02T)$ pulses/sec, where T is the 9-bit scaler content. Although the *S–T* scaler has a better dynamic range than an *S* scaler of the same

© Kluwer Academic Publishers • Provided by the NASA Astrophysics Data System

1971SoPh...17..218B

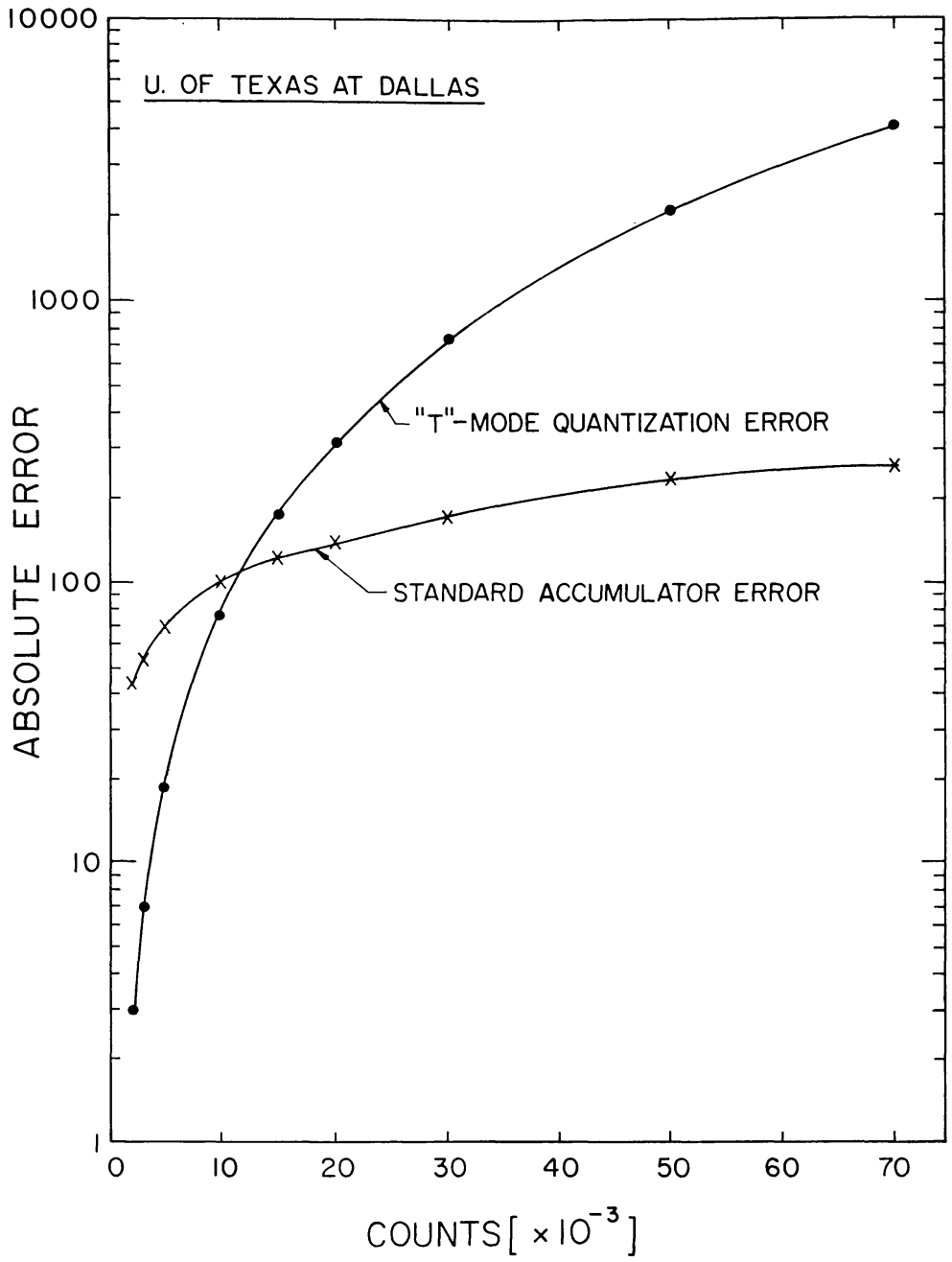

Fig. 7. The absolute quantization error of an *S–T* type accumulator operating in the *T*-mode, as a function of the input counting rate. The absolute error of a standard accumulator is also shown.

number of bits, the quantization errors are large compared to the statistical errors at high counting rates, as is shown in Figure 7. The scalers are effectively set to zeros at the end of each freeze period.

6. Anisotropy Measurements

During the anisotropic mode, pulses from the appropriate detector logic are routed to one of eight spacecraft accumulators (defined as SCA 1–8) as determined by the

© Kluwer Academic Publishers • Provided by the NASA Astrophysics Data System

1971SoPh...17..218B

azimuth of the detector axis at the time of the measurement. Effectively, as the spacecraft rotates with respect to the Sun, the experiment subdivides a great circle in the ecliptic plane into eight equal accumulation time sectors. The particles detected in any given sector are counted by a corresponding scaler.

The spacecraft supplies an aspect signal consisting of 64 pulses spaced at rigorously equal intervals over each revolution plus a dead time pulse defining a short, variable, period of time used to accommodate small variations in the spacecraft spin period. This aspect signal, generated in a fashion similar to the scheme described by Bartley

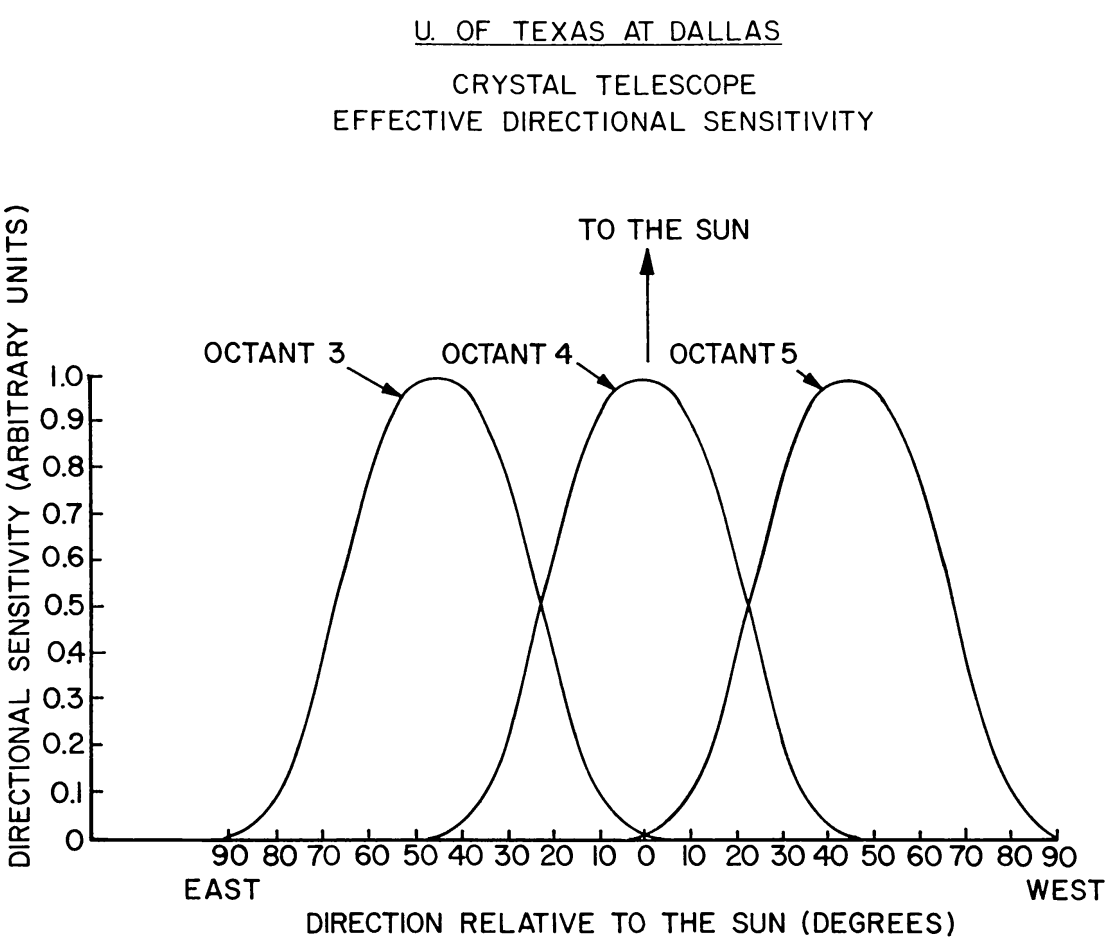

Fig. 8a. The directional sensitivity in arbitrary units of octants 3, 4, and 5 for the crystal telescope as a function of the angular separation from the Earth-Sun line.

et al. (1967b), is used to step the anisotropic routing through eight accumulator positions. Time accuracies for the aspect signal of better than one part of 10^4 are similarly achieved. This is important if the total number of counts in the Nth scaler is to be related to a flux from the Nth octant in space. To ensure accuracy, and to simplify the timekeeping problem, the experiment has been implemented such that only data from an integral number of octants will be accumulated into any given scaler, SCA 1–8. As mentioned above, the pre-freeze signal provides an appropriate warning to the

© Kluwer Academic Publishers • Provided by the NASA Astrophysics Data System

1971SoPh...17..218B

logic to inhibit data at the end of a completed octant prior to the readout period.

For each measurement the SCA-10 scaler contains two 3-bit words of information on the octant in which data taking began and the octant after which data taking ceased, i.e., 'START/STOP' data. From this, the particle counts recorded in each of the anisotropy scalers, SCA-1 to 8, can be normalized to the same number of octants (note that the total number of octants accumulated in any 9.28 sec. time period varies from interval to interval).

The optical aspect sensor, which maintains Sun synchronization of the aspect signal

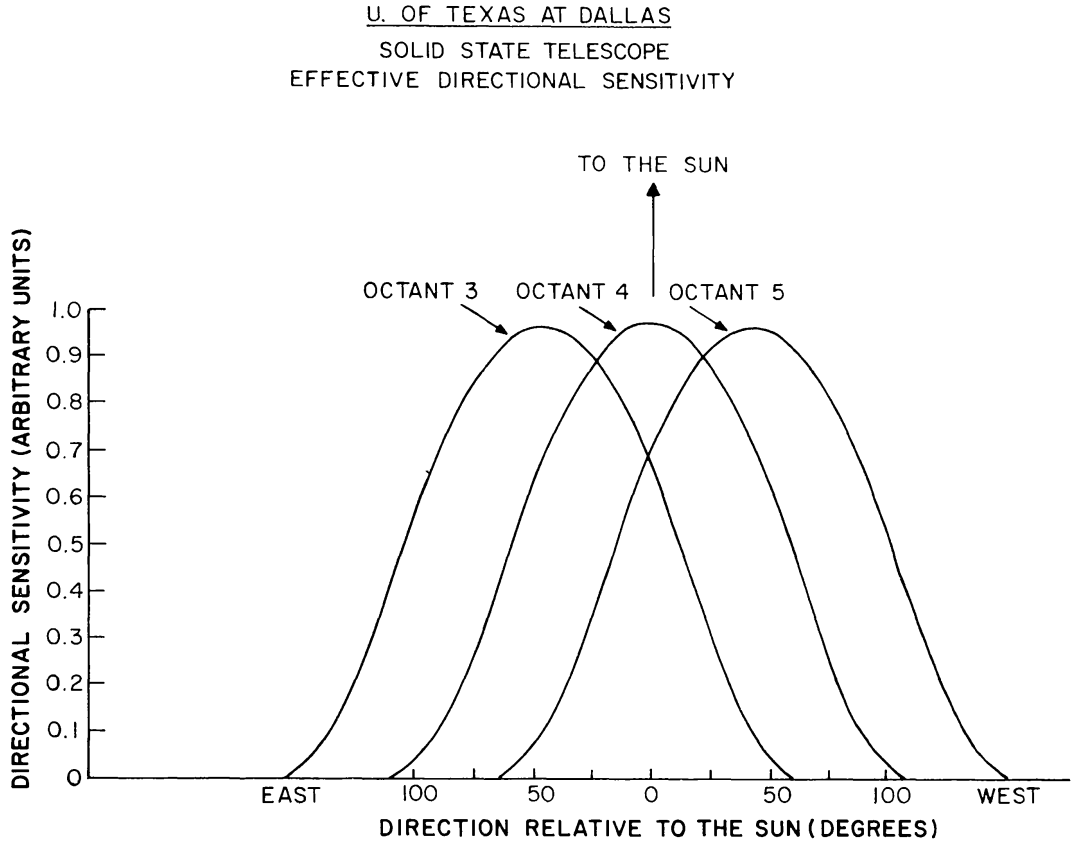

Fig. 8b. Same as Figure 8a for the solid state detector.

on Explorer 34, has a 'look' direction at an angle of 135° with respect to the detector axis. This phasing is taken into account when relating the anisotropy data generated by the instrument to the eight octants in space (see Figure 1 in next paper, p. 243). It will be noted in this figure that the 'look' direction of octant 4 is centered on the Sun-Earth line while the center of octant 1 contains the small variable dead time period (accumulation time for octant 1, however, is exactly equal to that for the other seven octants). As noted above the logic in the instrument is designed to ensure that during any 9.28 sec accumulation period, the number of times that each direction has been sampled is accurately known. With a satellite spin period of approximately 2.5 sec, each octant is sampled at least 3 times during each accumulation period.

© Kluwer Academic Publishers • Provided by the NASA Astrophysics Data System

1971SoPh...17..218B

Figure 8a shows the directional sensitivity for the telescope combination $BC\bar{D}$; Figure 8b shows the same for the $A\bar{B}$ logic. Figures 8c and 8d show the directional sensitivity for the proportional counter for electrons and protons respectively. These curves were obtained using the geometrical sensitivity of the detector and the azimuthal sectors shown in Figure 1 in next paper, p. 243.

To provide a quantitative description of the cosmic ray flux as a function of direction, a sinusoid of the form

$$Y = A_0 + A_1 \cos(\theta + \theta_1) + A_2 \cos(2\theta + \theta_2)$$

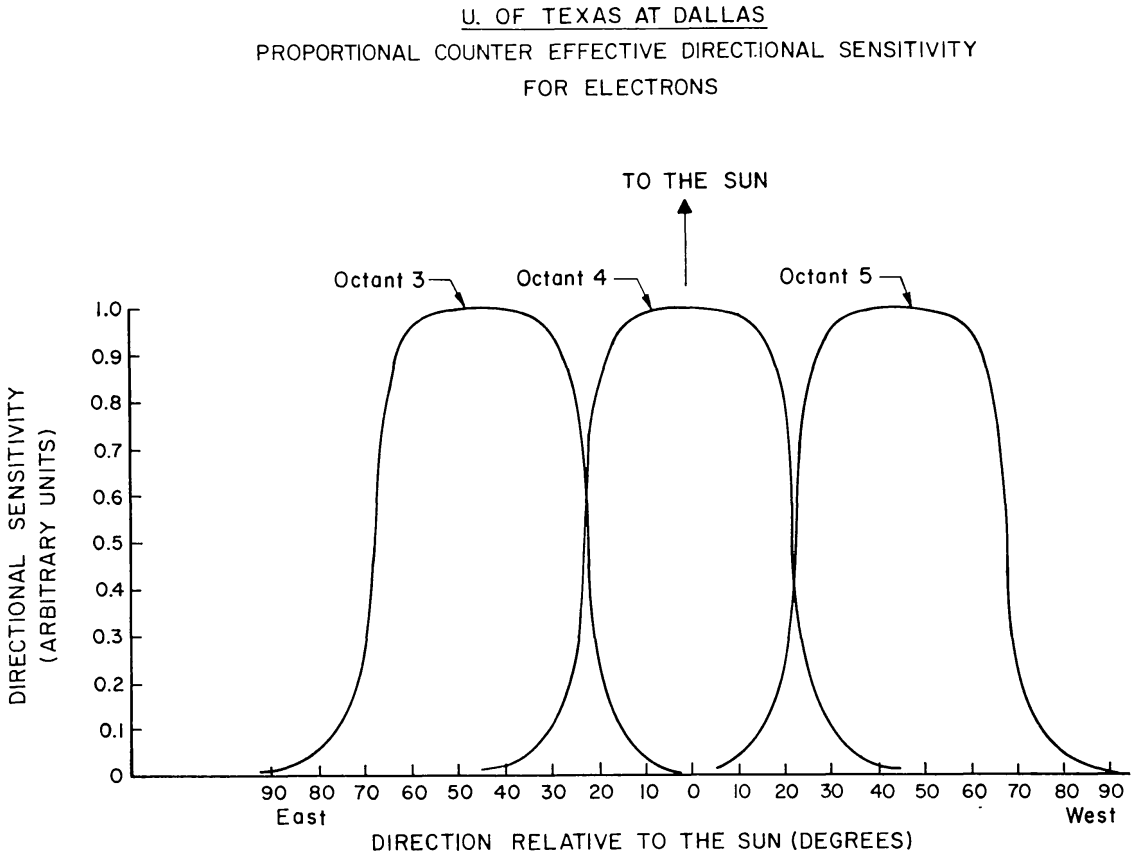

Fig. 8c. Same as Figure 8a for the proportional counter (electrons).

is fitted to each set of 8 data points taken during an anisotropy measurement. The true relative amplitude and phase of the first harmonic are given by $1.026 \times A_1/A_0$ and θ_1 respectively. The calculation of these quantities are outlined in Figure 9.

The sinusoidal fit is a convenient first order approximation to the actual picture. Detailed studies have shown that the sinusoidal fit provides a reasonable description even for cases of unidirectional anisotropy. The determination of the actual angular distribution of the radiation, using the known angular response of the detector, provides a result for the anisotropy azimuth seldom differing by more than 5° from the result obtained by a sinusoidal fit. It is more convenient to express the phase of

© Kluwer Academic Publishers • Provided by the NASA Astrophysics Data System

1971SoPh...17..218B

any anisotropy relative to the Sun-Earth line and this transformation is also given in Figure 9. Φ is the direction relative to the Earth-Sun line along which an observer must look to see the maximum cosmic ray flux. The example shown in Figure 9 is the fit for the low-energy proton data for 2100 UT on 2 November, 1967, for which the azimuth of the anisotropy is found to be 29° West of the Earth-Sun line.

In the calculations of azimuthal phase and amplitude for charged particle fluxes based on the proportional counter information contained in the accumulators SCA-1 to 8, data in octant 4 are discarded because of solar X-ray contamination. For anisotropy calculation purposes, pseudo-octant 4 data are generated by averaging the responses recorded in octants 3 and 5.

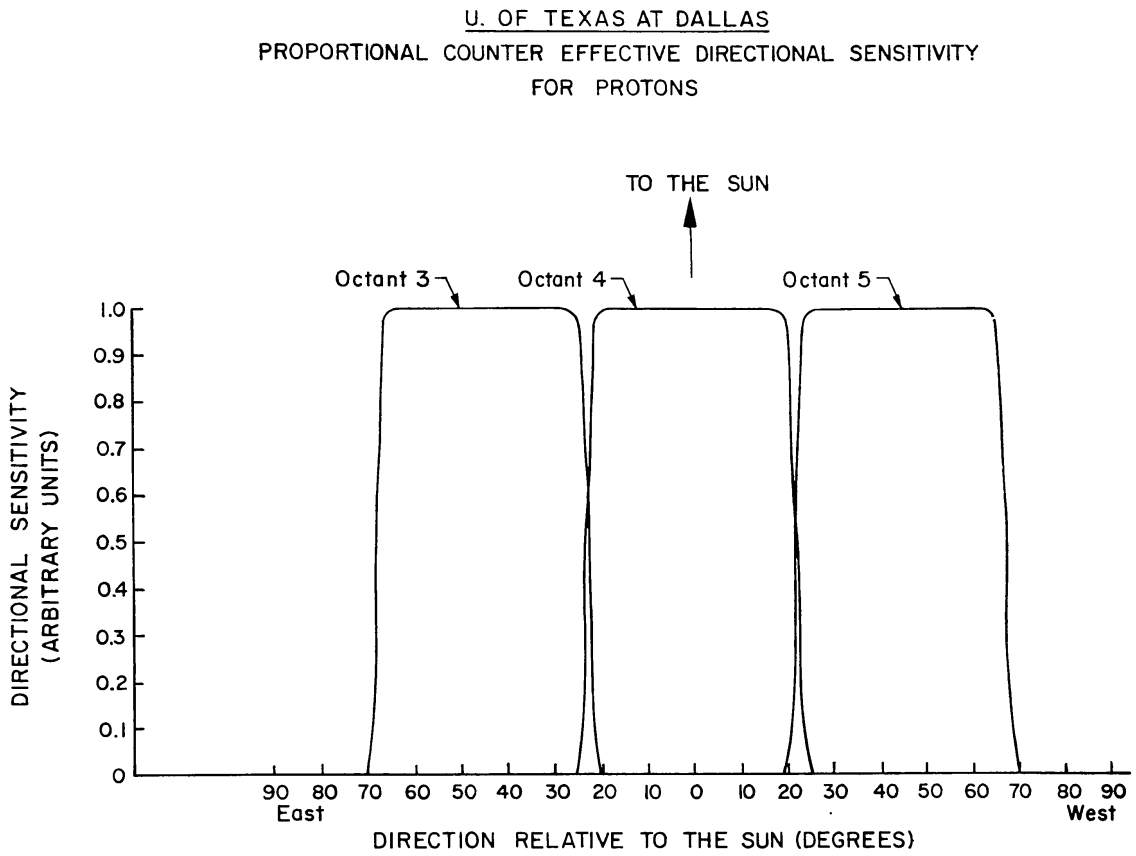

Fig. 8d. Same as Figure 8a for the proportional counter (protons).

7. Isotropic Measurements

During isotropic observations (refer to Figure 5) the output of each pulse height analyzer channel is continuously connected to an accumulator SCA-N ($1 \leqslant N \leqslant 7$). During these measurements the logics CD and AD are fed to SCA-8, accumulation occurring at all times other than during the freeze signal.

© Kluwer Academic Publishers • Provided by the NASA Astrophysics Data System

1971SoPh...17..218B

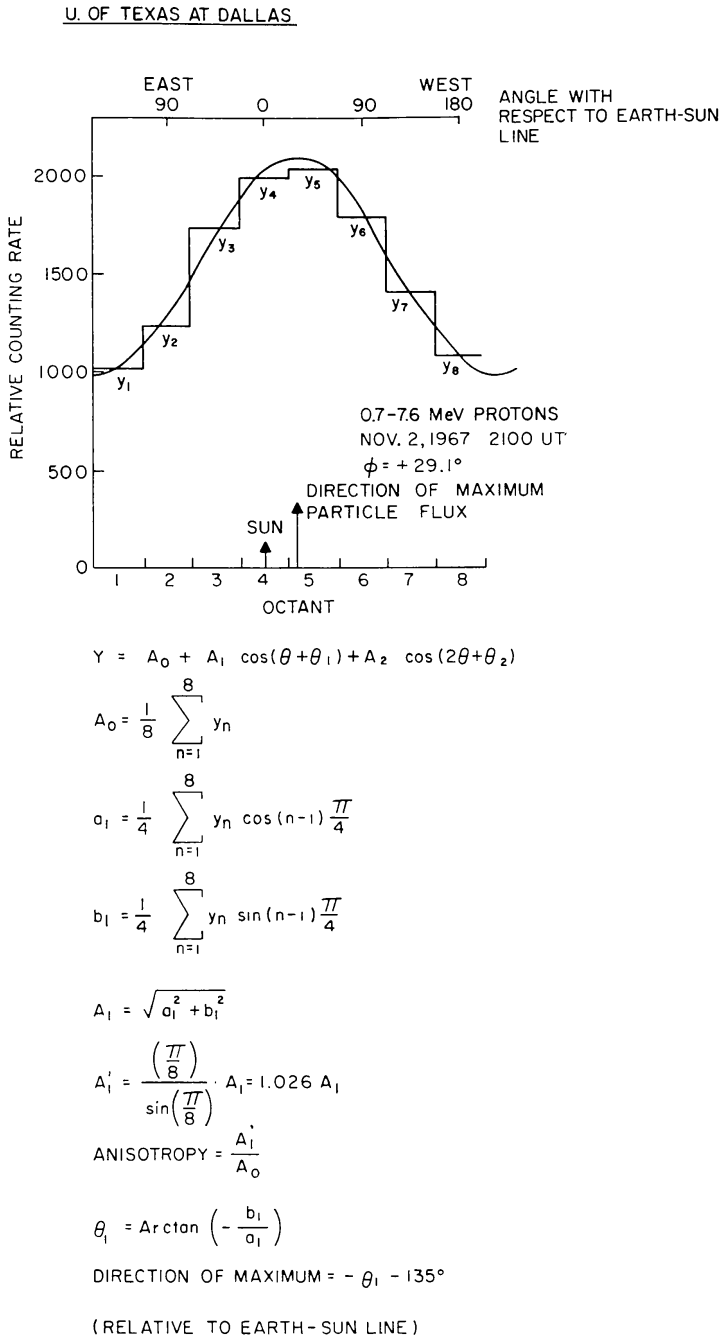

Fig. 9. Illustrating the sinusoidal fit and the calculation of the amplitude and direction of the anisotropy from the eight directional counting rates.

8. Post-Flight Calibration

During measurement 77 (octal), which is the last measurement of the complete sub-multiplexing schedule, the experiment performs a pulse height analysis of all pulses from the *C* scintillator. For this measurement, a unity attenuator is employed so that the six differential pulse height analyzer channels cover the energy range 1–9 MeV. The 10 nanocurie Am^{241} radioactive source attached to the *C* scintillator provides

© Kluwer Academic Publishers • Provided by the NASA Astrophysics Data System

1971SoPh...17..218B

5.5 MeV alpha particles for an inflight check of the stability of the complete system (high voltage, photomultiplier, amplifiers and discriminators combined). An analysis of the Am^{241} pulse height distribution obtained throughout the 23 months of operation has indicated that the overall stability of the complete crystal system was maintained, the maximum change corresponding to a decrease in the equivalent threshold of 10%. In addition, as mentioned above, Scaler 9 records the raw counting rates of the four telescope elements *A*, *B*, *C*, and *D* pre-scaled by a factor of 16. These rates could also be used to monitor the overall performance of the telescopes. Over the 23 months of operation, the quiet time counting rate of the *C* crystal decreased by 17% and that of the solid state by 33%. The 10% decrease in the equivalent threshold would have produced an increase of less than $<0.1\%$ in the raw counting rate of the *C* crystal. Consequently, the 17% and 33% changes noted above must be completely due to the 'eleven year' change in the cosmic ray flux in the solar system. During the same period the high energy cosmic rays ($>10^9$ eV) measured by the Churchill neutron monitor showed a long term decrease of $\sim 3\%$.

9. Identification of Proportional Counter Events

The proportional counter responds to X-rays, electrons, and protons. A solar X-ray event, however, due to X-rays emitted in the solar corona is highly anisotropic, and almost all the flux is received in octant 4 centered around the Sun direction. The presence of an increased flux from all octants serves to identify charged particle events. A simultaneous increase in the flux measured by the solid state detector is indicative of a proton event while an electron event causes an increase in the proportional counter counting rate, essentially without an accompanying increase in the solid state detector counting rate. The counting rate due to celestial X-rays, including Sco XR-1, is small and causes a negligible effect on the electron anisotropy measurements. Hence, it is usually possible to identify and measure three phases of solar flare events, first the solar X-ray burst, then the anisotropy and build-up of the electrons and finally, using the main charged particle telescope, the changes in the anisotropy and energy spectrum of the protons component.

10. Effect of the Earth's Field on Anisotropy Measurements

Anisotropy measurements in the vicinity of the Earth's magnetospheric boundary can be severely affected since the magnetosphere acts as a good reflector of low energy particles. Montgomery and Singer (1969) find that the cosmic-ray flux inside the magnetotail or within $\sim 1\ R_E$ of the magnetopause were much more isotropic than those farther from the magnetopause or in the interplanetary medium. In order to make a quantitative estimate of the effect of the magnetosphere on Explorer 34 anisotropy measurements (Explorer 34 goes through the magnetosphere approximately every 4.5 days), we have investigated the manner in which the angular distribution

© Kluwer Academic Publishers • Provided by the NASA Astrophysics Data System

1971SoPh...17..218B

of low energy cosmic ray particles of solar origin changes for two different cases of magnetospheric crossing:

(a) During 28–29 May, 1967, when the satellite line of apsides was at ~90° East of the Earth-Sun line.

(b) During 16–18 December, 1967, when the satellite line of apsides was at ~90° West of the Earth-Sun line.

Figures 10a and 10b show the observed amplitudes and phases of the first harmonic

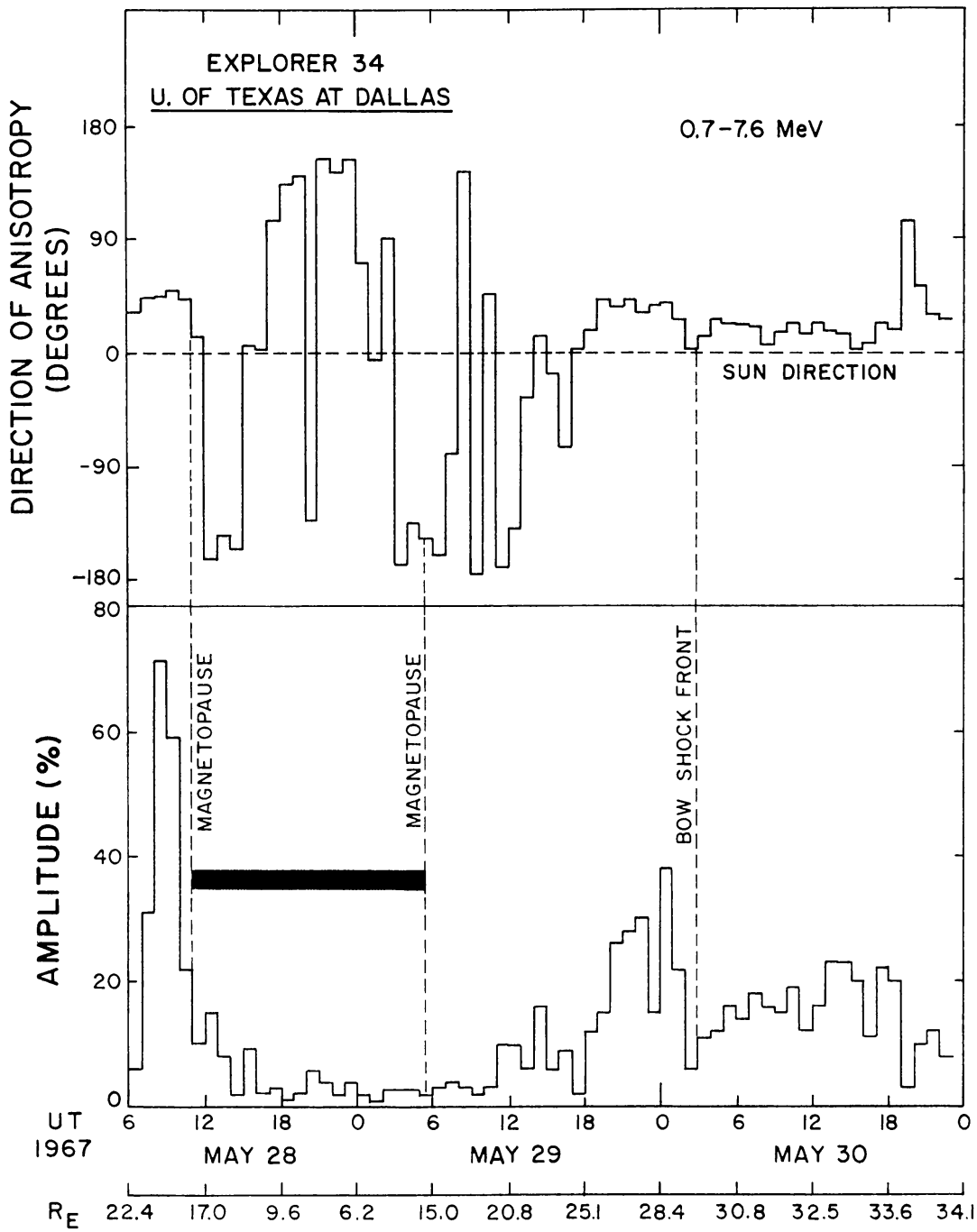

Fig. 10a

© Kluwer Academic Publishers • Provided by the NASA Astrophysics Data System

1971SoPh...17..218B

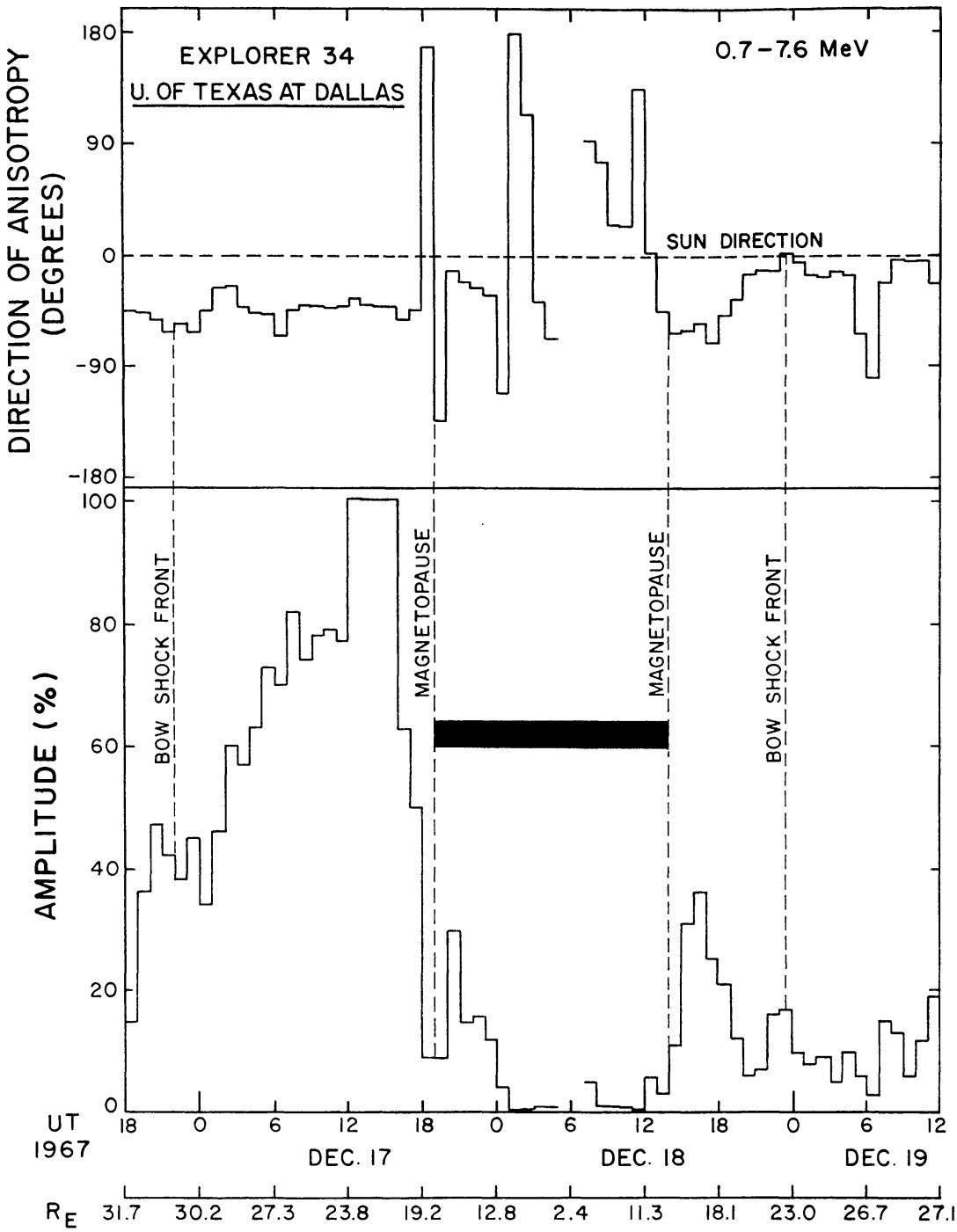

Fig. 10b

Fig. 10. Illustrating the dramatic reduction in anisotropy of low energy solar cosmic rays within the magnetosphere. The amplitude and direction of the anisotropy are plotted against time and geocentrical radial distance of the satellite for a) the 1967, May 28–30 event, and b) for the 1967, December 16–19 event. The position of the magnetopause and the bow shock front are indicated.

© Kluwer Academic Publishers • Provided by the NASA Astrophysics Data System

1971SoPh...17..218B

of the anisotropy of the solar particle fluxes for these two events. The radial distance from the center of the Earth is also marked in the horizontal scale. The time of crossing the bow shock front and the magnetopause are included in these diagrams (D. H. Fairfield, private communication). It can be seen from these figures that in both events, the amplitude of the anisotropy decreases sharply at the time of the inbound magnetopause crossing. At the time of the outbound magnetopause crossing the amplitude increases again although not so sharply, and it does not reach the original level. However, since the amplitude of the anisotropy during a solar event has been shown to decrease with time, the smaller anisotropy detected after the outbound crossing is most probably due to a temporal variation. Inside the magnetosphere, and consistently with the very small observed anisotropy, the phase of the first harmonic shows a very large variability, but it returns to the original value after the outbound magnetopause crossing. Care must therefore be exercised when interpreting solar cosmic ray anisotropies when the satellite is inside the magnetosphere. These anisotropies represent at best lower limits of the true anisotropy. Since, however, the Explorer 34 satellite has a highly eccentric orbit, spending more than 70% of its total time beyond $20R_E$, a large fraction of the anisotropy data is relevant to interplanetary space studies.

11. Effect of the Earth's Field on Spectral Measurements

We have also investigated the way in which the measured energy spectrum of solar cosmic rays depends on the satellite position with respect to the magnetopause. Figure 11 summarizes the results of this analysis for the solar flare events that occurred during the period 24 May, 1967–31 December, 1968. The upper part of Figure 11 shows the frequency distribution of occurrence of the exponent of the energy spectrum γ (assuming an spectral law of the form $\mathrm{d}J/\mathrm{d}E \propto E^{-\gamma}$), for all the events when the satellite was in the interplanetary medium. The distribution in this case seems to be flat, all exponents γ from 0.5 to 4.0 occurring with practically equal probability.

The frequency distribution when the satellite is inside the magnetosphere (depicted in the lower part of Figure 11) is markedly different. Values of $\gamma < 1.5$ are almost completely excluded. This, coupled with a decrease in the frequency of occurrence with increasing γ, produces a maximum in the distribution for values of γ between 1.5 and 2.0. The magnetosphere is seen then to modify the energy spectrum measurements in two ways, such that the most probable value of the exponent γ is between 1.5 and 2.0. It is thus clear that the low energy spectral measurements obtained when the satellite is inside the magnetosphere are not directly related to the properties of the interplanetary medium. Similar conclusion was reached in the preceding section concerning the anisotropy measurements.

12. Epilogue

In this paper, we have described a detector designed to measure the anisotropy and

© Kluwer Academic Publishers • Provided by the NASA Astrophysics Data System

1971SoPh...17..218B

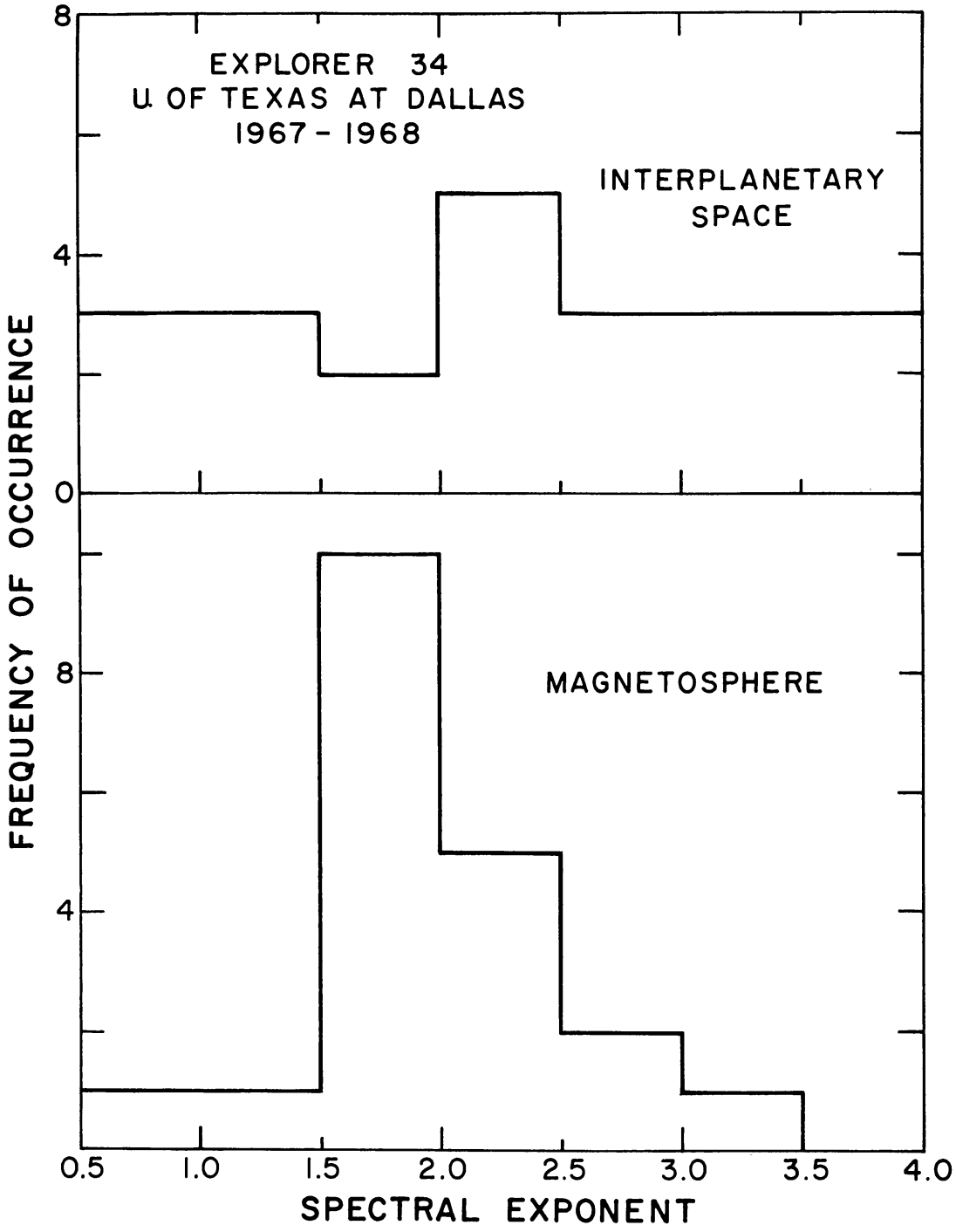

Fig. 11. Frequency distribution of the exponent of the energy spectrum for solar cosmic ray events detected in interplanetary space and inside the magnetosphere.

energy spectrum of the low energy electron and proton cosmic ray flux, and to investigate the properties of solar and galactic sources of X-rays in the range 2.7–8.6 keV. During the 23 months of the Explorer 34 life-time, the detector performed well, with the exception of the proportional counter which failed after 10 months of operation. The overall stability of the crystal detector system, for which

© Kluwer Academic Publishers • Provided by the NASA Astrophysics Data System

1971SoPh...17..218B

an in-flight calibration was provided, was shown to have remained constant to within 10%. The change in counting rate of the crystal detector due to this small gain change was shown to be less than 0.1%. The effect of the magnetosphere on the anisotropy of the solar cosmic ray was illustrated for two events, the main conclusion being that at the time of the magnetopause crossing the amplitude of the anisotropy decreases sharply to a very small value. The spectral characteristic of low energy solar cosmic rays, obtained when the satellite was inside the magnetosphere was shown to be markedly different from that obtained when the satellite was in the interplanetary medium.

Some conclusions drawn from data obtained from this detector concerning interplanetary propagation of electrons and protons are presented elsewhere.

Acknowledgements

We would like to thank Messrs. R. L. Bickel, J. Younse, W. Glasscock and D. W. Stang for designing the electronic circuitry for this detector. Thanks are also specially due to Messrs. R. H. Morgan, G. A. Stokes, B. W. LeFan, A. Bonham, B. Jenkins, L. D. Anschutz, P. T. Gronstal and to Mrs. A. B. Jourdan-Allum and M. Hopkins for crucial help provided during several phases of the construction, testing and integration of detector. The help provided by Mr. P. Butler, the IMP Project Office Personnel, and the engineers and technicians of the Electro-Mechanical Research Company during the integration and launching phase of the Explorer 34 and 41 satellites is greatly appreciated.

This work was supported by the National Aeronautics and Space Administration Grant NASr-198 and contract NAS5-9075.

References

Bartley, W. C., McCracken, K. G., and Rao, U. R.: 1967a, *Rev. Sci. Instr.* **38**, 266.

Bartley, W. C., McCracken, K. C., and Rao, U. R.: 1967b, *IEEE Trans. Aerospace and Electronic Systems* **3**, 230.

Bukata, R. P., Keath, E. P., Younse, J. M., Bartley, W. C., McCracken, K. G., and Rao, U. R.: 1970, *IEEE Trans. Nuclear Science* (in press).

Coleman, J. A., Love, D. P., Trainor, J. H., and Williams, D. J.: 1968, *IEEE Trans. Nuclear Science* **15**, 482.

Kanter, V. H.: 1967, *Ann. Physik* **20**, 144.

Montgomery, M. D. and Singer, S.: 1969, *J. Geophys. Res.* **74**, 2869.

© Kluwer Academic Publishers • Provided by the NASA Astrophysics Data System